



Extending the Life of Aircraft with Vapor Phase Inhibitors

Prepared for:

The Cortec Corporation

4119 White Bear Parkway

St Paul, MN 55110

(Report #1138)

Prepared by:

Behzad Bavarian, PhD

Professor of Materials Engineering

Lisa Reiner & Hamed Youssefpour

Dept. of Manufacturing Systems Engineering & Management

College of Engineering and Computer Science

California State University, Northridge

September 2004

Localized corrosion of Al-alloys in the aircraft industry can cause expensive catastrophic failures, especially in aging aircraft. The aluminum aircraft parts that are sensitive to stress corrosion cracking, if subjected to stresses and a corrosive environment, can have rapid failure with no warning. To further aggravate conditions, aircraft maintenance with conventional cleaning solutions can gradually destroy the protective aluminum oxide film and accelerate corrosion in crevices and lap joints. VCI 415, a solution with corrosion inhibition properties used for washing/rinsing aircraft was investigated to determine the corrosion susceptibility for several aluminum alloys (2024, 6061 and 7075). The VCI 415 chemical composition, as determined from XPS analysis, is a mixture of sodium compounds and hydrocarbon surfactant with uniform chemistry across the surface and minor variation of concentration with depth. Effectiveness of the inhibitor was confirmed with electrochemical impedance spectroscopy and elevated temperature studies. Polarization resistance increased with concentration of VCI 415, due to the film forming process and displacement of water molecules. As well, identification of the adsorption mechanism and corrosion activation energy was explored. Polarization behavior was consistent with Langmuir adsorption isotherms and the activation energy was increased from 29 kJ/mol (no inhibitor) to 37 kJ/mol for a solution containing 2000 ppm VCI 415. Cyclic polarization behavior for samples in the vapor phase inhibitor showed a shift in the passive film breakdown potential by roughly +600 mV, indicating an altered electrochemistry. The substantial increase in the passivation range has favorable consequences for pitting and localized cell chemistry. Crevice corrosion results showed improved corrosion inhibition behavior compared with samples tested in tap water only. The strain at failure and tensile strength from the stress corrosion cracking studies showed pronounced effects at -300mV; the fractographs showed an improved morphology with ductile overload as the primary failure mode. The inhibitor demonstrated an effective protective film on the surface of aluminum alloys with no adverse effects from the alkaline chemistry.

Introduction

Aluminum alloys that contain copper, zinc and magnesium as alloying elements have great importance for the aging aircraft community. One of the major concerns for the airline industry is maintaining this aging fleet of aircraft beyond their design life of 20 years. According to data presented in the 1999 edition of the Aviation & Aerospace Almanac, close to 7500 aircraft were operated by U.S. airlines in 1998 [1]. Some of these aircraft (B-727, DC-10) have been in service since the 1960s, when minimal attention was paid to corrosion. For the aircraft manufactured in the 1970s and 1980s, some corrosion control had been incorporated into the aircraft design (B-737, MD-81 and F-100), but damage tolerance was the primary concern. As the years passed, aircraft corrosion was becoming an economic burden and even endangering structural integrity. As part of the durability standards, airframe manufacturers began to use corrosion inhibiting primers and sealants for the faying surfaces of lap joints and fastener holes. Moreover, the Federal Aviation Administration (FAA) issued Airworthiness Directives (AD) related to corrosion control in design and maintenance [2]. By 1996, the total annual cost of corrosion for the U.S. aircraft industry was estimated at \$2.225 billion; further itemization shows that design and manufacturing cost \$0.225 billion, corrosion maintenance costs \$1.7 billion, and downtime due to corrosion was \$0.3 billion. With the

availability of new corrosion resistant materials and an increased awareness of the impact of corrosion on the integrity and operation of jet aircraft, the current design life of 20 years can be extended without jeopardizing structural integrity and significantly increasing the cost of operations [2]. Yet there is still reluctance to use the new materials in aircraft designs.

Stress Corrosion Cracking (SCC)

The primary use of high strength aluminum alloys is in aircraft construction; the airframe of modern aircraft is approximately 80 percent aluminum by weight [3, 4]. Some of the main reasons for selecting an alloy for aircraft applications are corrosion resistance, cost, and appearance. Traditionally, the structural aluminum alloys in aircraft have been 2024 in damage critical areas and 7075 in strength critical areas [5, 6]. In the past, when the aircraft was constructed largely of metal, skins were very thin and systems were rapidly replaced due to obsolescence, SCC problems were rare. However, when aircraft structures became more complex and skin materials became integral parts of the structure, SCC became more prevalent [7]. The high performance aircraft designed since 1945 have made extensive use of skin structures machined from thick plates and extrusions [8]. The residual stresses induced by the heat treatment in conjunction with those from the machining process made these materials sensitive to SCC [7]. Maintenance requirements increased as a result and development of higher strength alloys with improved resistance to corrosion without cladding began. The internal structure is comprised of stringers, spars, bulkheads, chord members and various fittings made of aluminum extrusions, honeycomb sandwiches, formed sheet, forgings and castings [8]. Aluminum alloys 7075-T6 and 2024-T3 (susceptible to both corrosion and SCC) are commonly used despite the availability of more corrosion resistant aluminum alloys with equal strength and fatigue properties [2].

The heat treatment or natural aging of materials induces residual stresses in these susceptible alloys that combine with operational loading stresses. A structure that has SCC sensitivity, if subjected to stresses and then exposed to a corrosive environment, may initiate cracks and crack growth well below the yield strength of the metal. What makes SCC difficult to manage is that failures occur along grain boundaries within the metal. Consequently, no corrosion products are visible, making it difficult to detect or prevent [7]. Fine cracks can penetrate deeply into the part. In Al-alloys and low-carbon steels, intergranular fracture is common. Some fractures show progression marks (easily confused with fatigue) and alternating regions of SCC and overload fracture. Aluminum alloys that contain appreciable amounts of soluble copper, magnesium, silicon and zinc are susceptible to SCC (Table 1) [9-11]. SCC is normally not a problem in the AlMgSi alloys unless the quenching rate has been too slow, but even then only under high transverse stress. AlMg alloys with more than 4% Mg and high strength alloys from the 2000 or 7000 series can experience SCC [12]. SCC isn't restricted to aluminum alloys though, other materials including high strength steels used in landing gear assemblies, can also fail by SCC [7]. The service record of 6000 series alloys shows no reported cases of SCC. In laboratory tests, however, at high stresses and in aggressive solutions, cracking has been demonstrated for particularly high silicon or copper content [9]. Stress corrosion cracking in aluminum alloys is characteristically intergranular. From an

electrochemical perspective, this requires anodic grain boundaries with respect to the rest of the microstructure resulting in selective attack of grain boundaries or closely adjacent regions without appreciable attack of the grains themselves. Intergranular corrosion is caused by potential differences between the grain-boundary region and the adjacent grain bodies. The location of the anodic path varies with the different alloy systems [9].

Corrosion in an aircraft can come in several forms; pitting and crevice corrosion are the most common forms in the 2000 and 7000 series of aluminum alloys, the principle materials of construction. Pitting corrosion produces deterioration of the airframe structures in localized areas and can have high penetration rates. Pits often create stress concentrations that may reduce the fatigue life of a component. Crevice corrosion is a localized form of corrosive attack that occurs at narrow openings or spaces between two surfaces (assuming at least one of them is a metal). A concentration cell forms with the crevice being depleted of oxygen. This differential aeration between the crevice (microenvironment) and the external surface (bulk environment) gives the crevice an anodic character. This can contribute to a highly corrosive condition in the crevice [13]. Both pitting and crevice corrosion can develop into exfoliation corrosion or intergranular stress corrosion cracking (IGSCC) that is common around fastener holes and plate edges. IGSCC occurs when stresses are applied perpendicular to the susceptible grain boundaries. More so than pitting and crevice corrosion, susceptibility to exfoliation corrosion and intergranular stress corrosion cracking depends on alloy type, heat treatment and grain orientation [2]. Traditionally, corrosion has not been given sufficient attention with respect to structural integrity, possibly due to complexities of the corrosion process and the inability to predict nucleation and growth behavior. Corrosion has not been incorporated into the damage tolerance assessments and as aircraft continue to age, corrosion will increasingly affect the structural integrity [2].

Table 1 - Chemical composition of several aircraft aluminum alloys [14].

| Alloy | Cu | Mg | Mn | Si | Fe | Ni | Cr | Zn | Ti | Al |
|----------------------|------------|------------|-------------|------------|------------|----|-------------|-------------|-------------|------------|
| AA6061 | 0.4 | 1.2 | 0.15 | 0.8 | 0.7 | - | 0.35 | 0.25 | 0.15 | Bal |
| AA7075 | 2.0 | 2.9 | 0.03 | 0.4 | 0.5 | - | 0.4 | 6.1 | 0.2 | Bal |
| AA2014 | 5.0 | 0.8 | 1.2 | 1.2 | 0.7 | - | 0.1 | 0.25 | 0.15 | Bal |
| AA2024 | 4.9 | 1.8 | 0.9 | 0.5 | 0.5 | - | 0.1 | 0.25 | - | Bal |
| AA7010 | 2.0 | 2.7 | 0.3 | 0.10 | 0.15 | - | 0.05 | 6.7 | - | Bal |
| Commercial purity Al | 0.2 | 0.05 | 0.05 | 1.0 | 0.4 | - | - | 0.1 | - | Bal |

Vapor phase corrosion inhibitors

Several groups of organic compounds have reported inhibitive effects for aluminum corrosion. The extent of adsorption of an inhibitor depends on many factors: (a) the nature and the surface charge of the metal; (b) the inhibitor adsorption mode; (c) the inhibitor's chemical structure; and (d) the type of aggressive solution. The presence of heteroatoms (oxygen, nitrogen, sulfur, phosphorus), triple bonds and aromatic rings in the

inhibitor's chemical structure enhance the adsorption process [16]. Coating to substrate adhesion and the diffusion of water and other species from an external environment to the coating/substrate interface are critical factors for the corrosion inhibition of organic protective coatings. Corrosion prevention systems commonly used in the military and commercial aviation fall into six basic categories: protective coatings (polyurethanes, epoxies); inorganic finishes (chrome, cadmium plating, anodizing); corrosion inhibitive compounds (water displacing oils); sealants (silicones, polysulfides); corrosion resistant alloys; and desiccants. Another possibility for aircraft protection is Volatile Corrosion Inhibitors (VCI) where protective vapors deposit on the exposed surfaces (including cracks and crevices) and condense to form a thin barrier of tiny crystals. The crystals dissolve when in contact with water, causing the adsorption of a monomolecular coating to the metal surface that helps repel water. VCI effectiveness, however, depends on package integrity and porosity, temperature, humidity, acidity and UV exposure [17].

VCI can be a complex mixture of amine salts and aromatic sulfonic acids that provide direct contact inhibition and incorporate volatile carboxylic acid salts as a vapor phase inhibitor for metal surfaces not sufficiently coated. The thin polar layer of surfactants is tightly bound to the metal surface through chemisorption. Between this thin polar layer and the corrosive environment is the thicker barrier layer of hydrocarbons. The sulfonate part of the inhibitor displaces water from the metal and is chemisorbed to the surface [18]. A surface active inhibitor component will be strongly chemisorbed or adsorbed at active sites having energy levels complimentary to the energy levels of the polar group, thereby forming a tighter, more uniform layer over the metal surface. The barrier layer has three important characteristics: 1) low permeability by moisture and other corrosives; 2) compatibility with the oleophilic ends of the polar layer molecules so that the barrier is held firmly in place; and 3) good solubility in the carrier to attach the polar and barrier layers to the metal surface [18]. The VCI film barrier replenishes through further evaporation and condensation of the inhibitor on the metal surface.

Aircraft maintenance

Aircraft components are frequently washed or rinsed during manufacturing and while in service to remove contaminants (salt, dirt, grease and oil). There are three main types of cleaning: aqueous, organic solvent, and abrasive. Aqueous cleaning covers a wide variety of cleaning methods (detergents, acids and alkaline compounds) to displace soil [15]. Improved corrosion prevention compounds and coating systems can isolate the sensitive alloy from the environment. This coupled with improvements to repair procedures will ensure adequate performance of a structure manufactured from a SCC sensitive alloy. The most costly, yet best method for eliminating SCC is to replace the material with an alloy specifically designed to resist this form of corrosion [7].

VpCI[®]-415 is a heavy-duty biodegradable water based alkaline cleaner and degreaser. The compounds contained in VpCI[®]-415 function by altering hydrocarbons (grease) so that the deposits can be removed with water. Any conventional equipment (power washers, steam cleaners, dip tanks) can be used for multimetal corrosion protection. Ethoxylated alcohols (C₉-C₁₁) [19], the active ingredient in the 415 inhibitor are based on short chain alcohols giving fast penetration of soil and improved performance on hard

surfaces. Narrow range alcohol ethoxylates, with two cloud points, allow the replacement of several nonionics in various formulations [20].

Adsorption Isotherms

It is assumed that the corrosion current density, which is directly related to the corrosion rate, is representative of the number of corrosion sites. Therefore, adding inhibitor to the environment should diminish the number of corrosion initiation sites by displacing water molecules on the surface with inhibitor molecules, thereby decreasing the corrosion rate. By measuring the corrosion current density of a solution with no inhibitor (blank) and an inhibited solution (or by measuring the polarization resistance), the surface coverage, θ , can be defined by the following formula:

$$\theta = \frac{I_{corr}(B) - I_{corr}(I)}{I_{corr}(B)} \quad \text{or} \quad \theta = \frac{\frac{1}{Rp(B)} - \frac{1}{Rp(I)}}{\frac{1}{Rp(B)}} \Rightarrow \theta = \frac{Rp(I) - Rp(B)}{Rp(I)} \quad (1)$$

where $I_{corr}(B)$ and $Rp(B)$ are the corrosion current and polarization resistance of the blank solution, respectively. $I_{corr}(I)$ and $Rp(I)$ are the corrosion current and polarization resistance for the inhibited solution, respectively. An adsorption isotherm is a mathematical function that relates the surface coverage of a chemical on a surface (usually a metal) to the concentration of the chemical. Identification of the surface adsorption isotherm is important in that it and classical thermodynamics can lead to the determination of a mechanism. In recent years, some indirect methods (electrochemical and weight loss) that relate the corrosive electric current density or the amount of weight loss with the inhibitor coverage have been used to study adsorption and the corrosion inhibition of various materials on a metallic surface [21, 22]. Many models for adsorption isotherms have been defined (Temkin, Freundlich, Langmuir and Frumkin). Each of these adsorption isotherms explains a different type of relationship between concentration and surface coverage of an inhibitor on a metal or alloy surface [23]. Based on the adsorption isotherm graph, the adsorption equilibrium constant, K_{ad} , can be calculated. Having the adsorption equilibrium constant, can lead to the calculation of the free standard energy of adsorption, $\Delta G_{ad} = -RT \ln(K_{ad})$. By repeating the same experiment at different temperatures, the enthalpy of the adsorption, ΔH_{ad} can be calculated from $\ln C = (\Delta H_{ad}^0/RT) + \text{Constant}$.

Experimental Procedures

Preliminary testing began with cyclic polarization per ASTM-G61 standards [24] to evaluate the electrochemical behavior. These techniques can provide useful information regarding the corrosion mechanisms, corrosion rate and corrosion susceptibility of the material for a given environment. Polarization methods involve changing the potential of the working electrode and monitoring the current that is produced as a function of time or potential. The studies were conducted using an EG&G VersaStat™ potentiostat with EG&G M352 DC corrosion test software. The aluminum alloys were tested in a solution of tap water plus 5% inhibitor. A standard platinum electrode was used with a platinum counter electrode in a 3-electrode configuration with the working electrode. Polarization scans were performed between -1.5 to 1.0 V relative to the open circuit potential. Also, a series of cyclic polarization tests were performed in temperatures ranging from 25 °C to

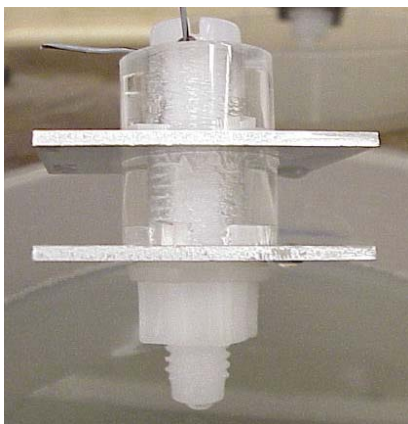
65 °C. These tests were performed to investigate the effect of temperature on the VCI/metal behavior. For the cyclic polarization tests, samples of aluminum 7075 were polished (600 grit sandpaper) and placed in an EG&G flat cell with a solution of 2000 ppm VCI 415, deionized water and 3.5 % NaCl.

To further investigate the (corrosion inhibition) effectiveness of VCI 415 on aluminum alloys and gather data for adsorption isotherms, flat samples from three classes of high strength aluminum alloys (2024, 6061 and 7075) were polished (600 grit sandpaper), placed in a flat cell and tested in a Gamry PC4/750TM Potentiostat/Galvanostat/ZRA using electrochemical impedance spectroscopy EIS300TM systems. Solutions containing tap water and 3.5% NaCl with varying concentrations of VCI 415 were prepared. Electrochemical impedance was measured by applying a sinusoidal signal to an electrochemical cell and measuring the current. The AC signal response to the system produces an AC signal with a phase shift and modified amplitude [25]. From the Bode plot, which is a curve that plots frequency vs. impedance, the polarization resistance, R_p , can be determined. The R_p is a convenient parameter that is inversely proportional to the current density and can be used to fit the data into an adsorption isotherm model.

Crevice Corrosion Investigation

The aluminum alloys were tested in an eight-station alternate immersion system. The samples (Table 2) were immersed in various concentrations of corrosion inhibitor, sodium chloride (NaCl) and tap water in the testing scheme as outlined in Table 2. Alternate immersion, an aggressive procedure, was performed to evaluate the inhibitor's ability to resist crevice corrosion. The testing cycle immersed the samples for 10 minutes, then exposed them to air for 50 minutes per ASTM G44 and G47 [26, 27]. After 500 hours of testing, the samples were taken apart, examined and photographed to document the crevice corrosion response.

Table 2 - Alternate Immersion testing schedule and photo of crevice sample.

| Alloy | VCI 415 | NaCl | water | hours | |
|-------|---------|-------|-------|-------|--|
| 7075 | 0% | - | tap | 500 |  |
| | 0% | 1.00% | tap | 500 | |
| | 5% | 1.00% | tap | 500 | |
| | 10% | 1.00% | tap | 500 | |
| 6061 | 0% | - | tap | 500 | |
| | 0% | 1.00% | tap | 500 | |
| | 5% | 1.00% | tap | 500 | |
| | 10% | 1.00% | tap | 500 | |
| 2024 | 0% | - | tap | 500 | |
| | 0% | 1.00% | tap | 500 | |
| | 5% | 1.00% | tap | 500 | |
| | 10% | 1.00% | tap | 500 | |

SCC Investigation

The slow strain rate tests were conducted on cylindrical samples (with a reduced cross sectional area) using a rate of $2 \times 10^{-7} \text{ sec}^{-1}$. Ten tests per alloy were completed to determine the effects of inhibitor and applied potentials on tensile strength and strain at failure. Table 8 summarizes the environmental conditions for the specimens. Based on these results the degree of SCC susceptibility was calculated.

X-ray Photoelectron Spectroscopy (XPS)

The Kratos AXIS ULTRA integrates a magnetic immersion lens, charge neutralization system, high performance hemispherical energy analyzer and a spherical mirror analyzer. The spherical mirror analyzer provides real time chemical state and elemental imaging using the full range of pass energies and multi-point analysis. The instrument's exceptional small spot spectroscopy capabilities (<15 microns) are achieved via a combination of the magnetic lens and selected area apertures. Monochromatic sources and charge neutralization guns have improved XPS capabilities for detecting variations in chemical composition and oxidation state. These subtle changes in peak positions and shape can supply significant information about the surface chemistry [28]. In XPS, the photon is absorbed by an atom in a molecule or solid ($A + h\nu \rightarrow A^+ + e^-$), leading to ionization and the emission of a core (inner shell) electron. The kinetic energy distribution of the emitted photoelectrons can be measured using an electron energy analyzer. Conservation of energy requires that: $E(A) + h\nu = E(A^+) + E(e^-)$. Since the electron's energy is in terms of kinetic energy (KE), the following expression for the KE of the photoelectron can be used: $KE = h\nu - [E(A^+) - E(A)]$. The final term in brackets, representing the difference in energy between the ionized and neutral atoms, is generally called the binding energy (BE) of the electron; $BE = h\nu - KE$. The binding energies for solids are conventionally measured with respect to the Fermi-level of the solid, rather than the vacuum level. This involves a small correction to the equation given above in order to account for the work function (Φ) of the solid, but for simplicity has been neglected [29]. The energy of the ejected photoelectrons can be measured to calculate the binding energy (the energy required to remove the electron from its atom). From the binding energy some important information like elemental components, relative composition, and chemical state can be determined for a given sample. Electrons can only escape from the solid if they originate close to the surface. If they are too deep within the bulk of the solid, they will be reabsorbed or undergo inelastic collisions. The information obtained from XPS is, therefore, highly surface sensitive [30]. The XPS analyses were conducted to access surface composition, depth profiling and the nature of inhibitor bonding to substrate surface.

Results

Cyclic Polarization Behavior

Figures 1-4 show the polarization behavior for the three alloys in tap water and inhibitor. Most noticeable is the positive shift in the breakdown potential by at least 600 mV. The inhibitor has altered the electrochemistry, increased the passivation range dramatically, and had beneficial consequences for pitting and localized cell chemistry. Figure 5 compares the breakdown potential for the VCI 415 and untreated samples; this bar graph chart clearly demonstrates the improvement in the breakdown potentials.

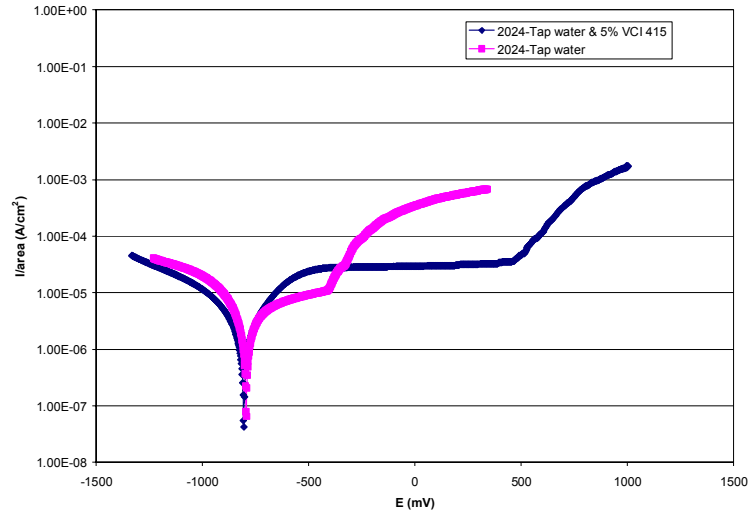


Figure 1: Comparison of polarization behavior for 2024 in tap water & VCI 415.

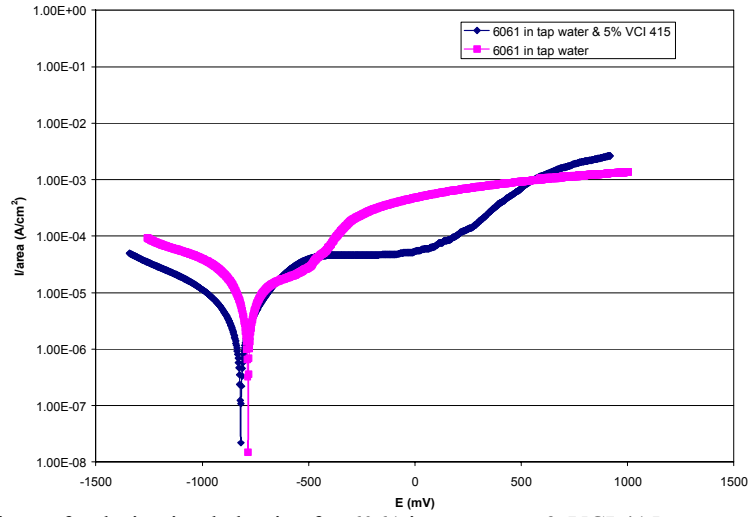


Figure 2: Comparison of polarization behavior for 6061 in tap water & VCI 415.

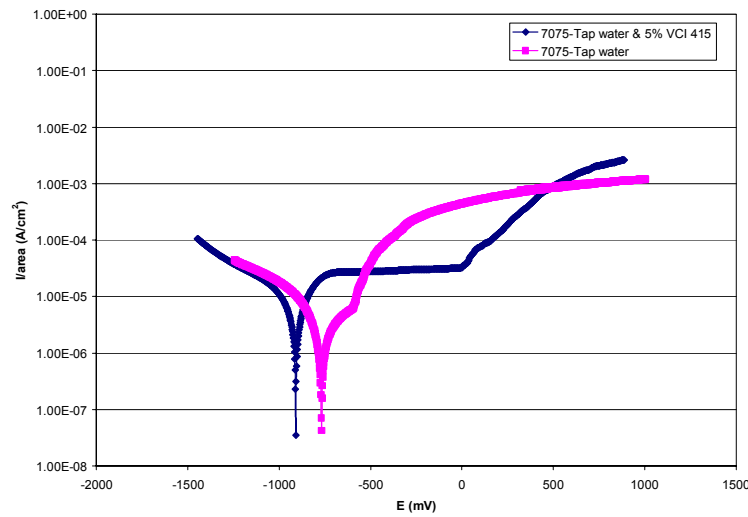


Figure 3: Comparison of polarization behavior for 7075 in tap water & VCI 415.

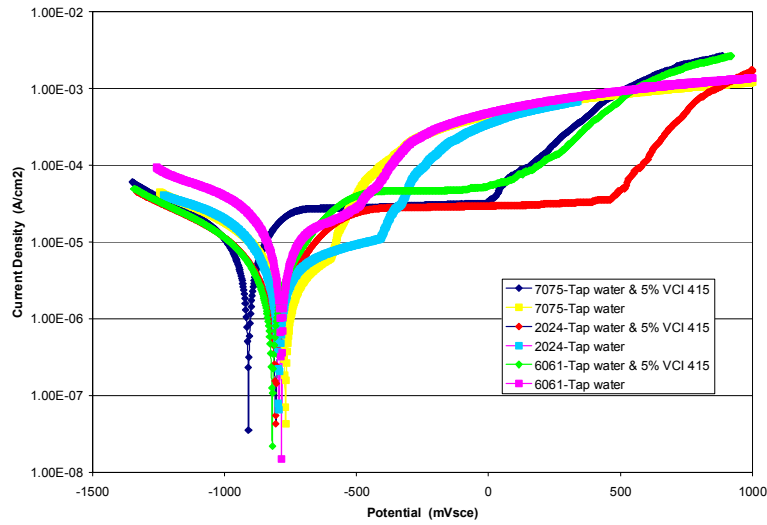


Figure 4: Electrochemical polarization behavior for Al-alloys in 5% VCI 415 solution per ASTM G61.

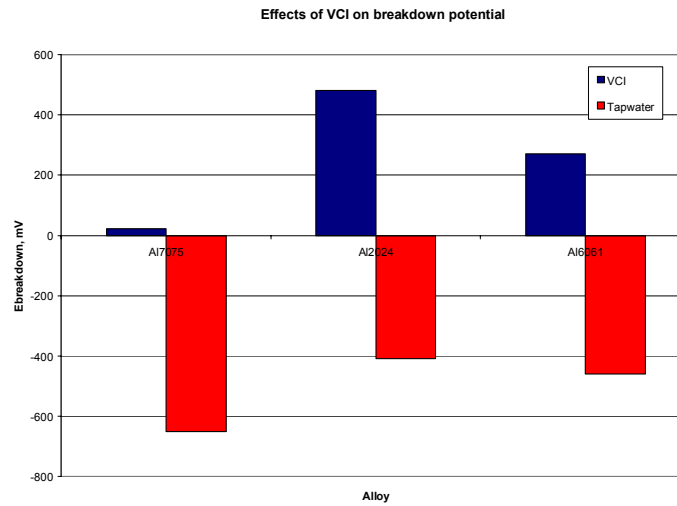


Figure 5: Bar graphs show the improvement in the breakdown potential for VCI 415.

Effect of temperature

To explore the activation energy of the corrosion process and the adsorption thermodynamics for the inhibitor, cyclic polarization was conducted in temperatures ranging from 35 - 65°C. Corresponding data are given in Table 3, graphed in Figure 6 and demonstrate the temperature dependence of I_{corr} and E_{corr} obtained in 2000 ppm VCI 415 and 3.5% solution with deionized water. The results show that the corrosion behavior of aluminum 7075 fluctuates with temperature. The increased temperature causes a more negative E_{corr} and also increases the I_{corr} .

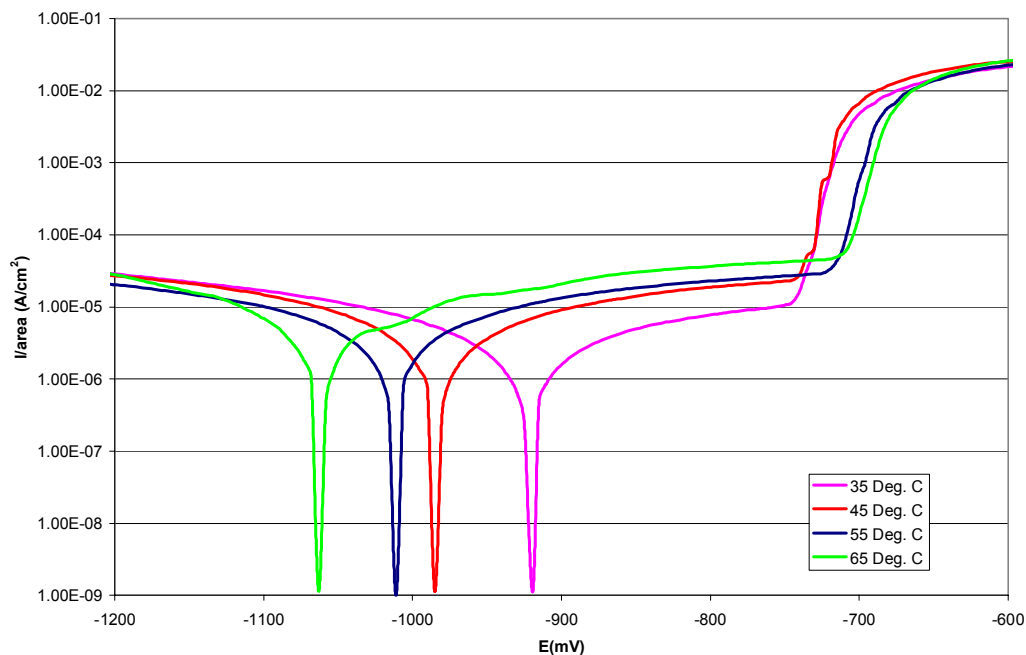


Figure 6: Cyclic polarization tests for Al-7075 in 2000 ppm VCI 415 and 3.5 % NaCl solution.

| Table 3 - Influence of temperature on electrochemical parameters for Al-7075. | | |
|---|------------------------|---|
| Solution of 2000 ppm VCI 415, 3.5% NaCl & deionized water. | | |
| Temperature (°C) | E_{corr} (mV) | I_{corr} ($\mu\text{A}/\text{cm}^2$) |
| 35 | -919 | 0.5 |
| 45 | -985 | 0.8 |
| 55 | -1011 | 1.0 |
| 65 | -1063 | 2.0 |
| Solution of 3.5% NaCl & deionized water. | | |
| Temperature (°C) | E_{corr} (mV) | I_{corr} ($\mu\text{A}/\text{cm}^2$) |
| 25 | -750 | 4.27 |
| 35 | -772 | 5.26 |
| 45 | -785 | 7.9 |
| 55 | -766 | 13.25 |
| 65 | -767 | 15.73 |

EIS, when modeled correctly, is a powerful tool for the analysis of complex electrochemical systems. A modified Randles model was used to obtain the polarization resistance (R_p) values. The Bode plots show that VCI 415 increases the polarization resistance of the Al-alloy samples (Figures 7-9) with higher inhibitor concentrations resulting in higher R_p values. The increased polarization resistance can be attributed to the film formation on the aluminum surfaces. Seen in Table 4 and Figures 7-9, the addition of inhibitor has increased the R_p value from 6 k Ω for Al-7075 in the blank solution (0 ppm concentration) to 134 k Ω for 5000 ppm VCI 415 in solution. For Al-6061, the increase is from 11 k Ω to 58 k Ω for 3000 ppm and for Al-2024, the increase was from 16.7 k Ω to 597 k Ω for 5000 ppm.

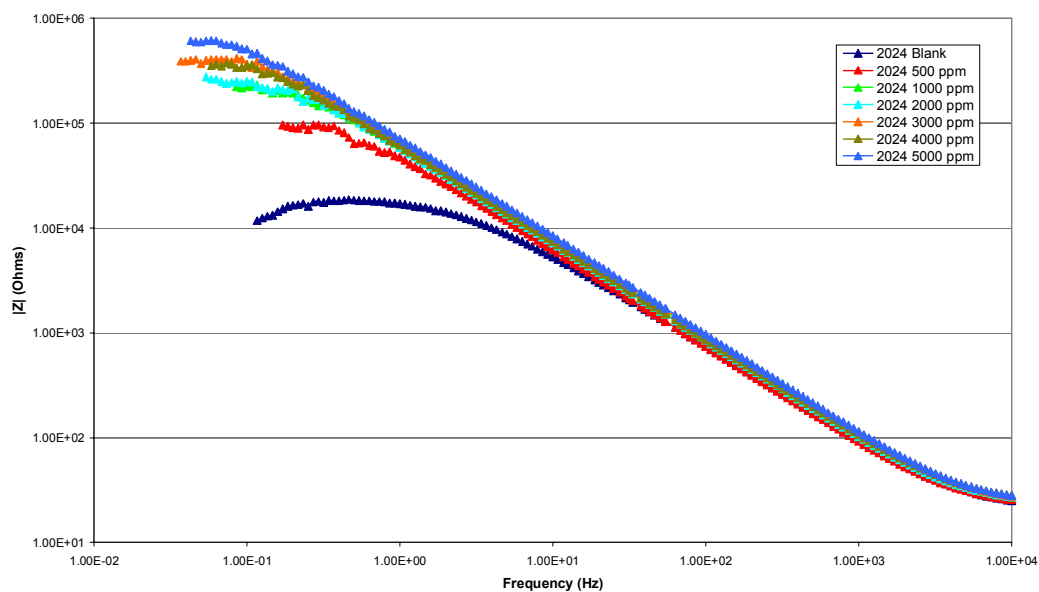


Figure 7: Bode plots obtained from AC impedance test of Al-alloy 2024 and various concentrations of inhibitor.

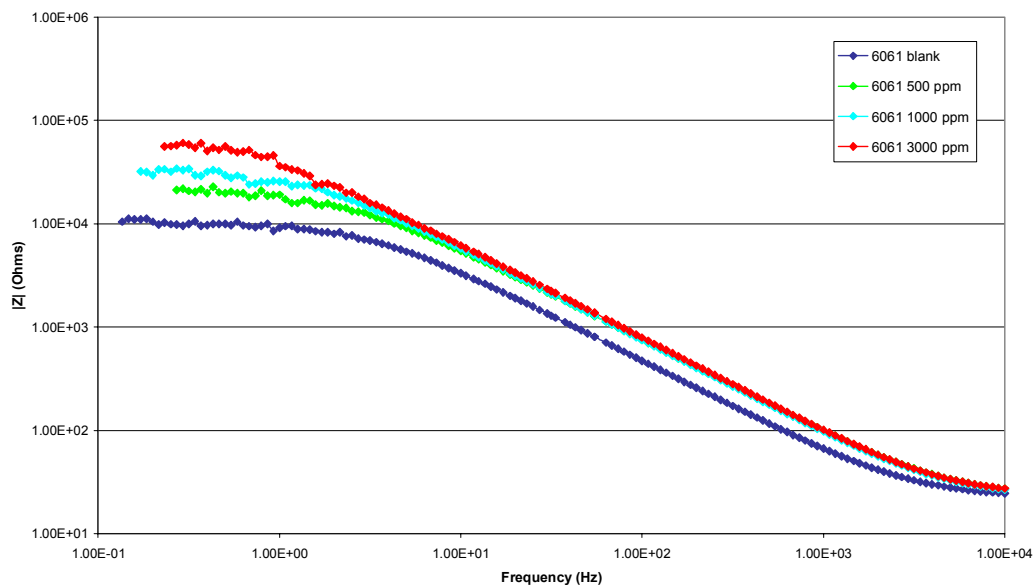


Figure 8: Bode plots obtained from AC impedance test of Al-alloy 6061 and various concentrations of inhibitor.

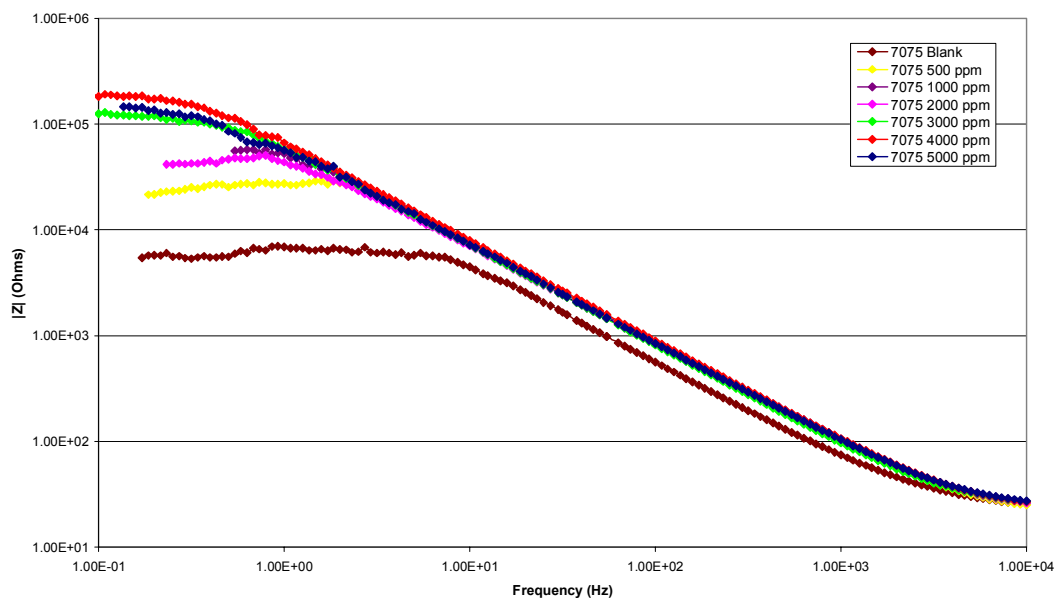





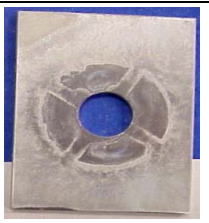
Figure 9: Bode plots obtained from AC impedance test of Al-alloy 7075 and various concentrations of inhibitor.





Table 4 - R_p values ($K\Omega$) for aluminum alloys from EIS

| Alloy | VCI 415 Concentration (ppm) | | | | | | |
|-------|-----------------------------|------|------|------|------|------|------|
| | 0 | 500 | 1000 | 2000 | 3000 | 4000 | 5000 |
| 2024 | 16.7 | 95.9 | 222 | 354 | 389 | 354 | 597 |
| 6061 | 11 | 21.9 | 33.5 | | 57.6 | | |
| 7075 | 6.04 | 24.6 | 55.8 | 43.3 | 126 | 189 | 134 |

Table 5 shows photos of Al-2024 after 500 hours of alternate immersion in various solutions. The sample immersed in one-percent NaCl shows the greatest corrosion damage. The addition of VCI 415 improved the corrosion resistance for this alloy. Similar results were obtained for Al-6061 (Table 6) and Al-7075 (Table 7).

Table 5 - Aluminum 2024 - Alternate Immersion – 500 Hrs

| | | | |
|---|-----------|--|---------------------------------------|
|  | 1% NaCl |  | 5% VCI 415, Tap water, 1% NaCl |
|  | Tap water |  | 10% VCI 415, Tap water, 1% NaCl |

| Table 6 - Aluminum 6061 - Alternate Immersion – 500 Hrs | | | |
|---|-----------|--|---------------------------------------|
|  | 1% NaCl |  | 5% VCI 415, Tap water, 1% NaCl |
|  | Tap water |  | 10% VCI 415, Tap water, 1% NaCl |





| Table 7 - Aluminum 7075 - Alternate Immersion – 500 Hrs | | | |
|--|-----------|---|---------------------------------------|
|  | 1% NaCl |  | 5% VCI 415, Tap water, 1% NaCl |
|  | Tap water |  | 10% VCI 415, Tap water, 1% NaCl |

Table 8 outlines the testing conditions and shows the numerical data for the tensile strength and strain at failure. Strain for 6061 and 7075 improved slightly for the samples tested in VCI. There was very little effect on tensile strength. Figures 10-12 show the data graphed in Excel and the comparisons of the stress/strain response. To evaluate the inhibitor's effectiveness, some alloys were tested in a 5% VCI solution (a typical concentration used for washing aircraft) and the reference samples were tested in tap water without inhibitor. Additionally, to determine the degree of effectiveness, potentials ranging from -700mV to -300 mV were applied to the samples during the SCC test. From the graphs in Figures 10-12, the greatest reduction in strain is seen in the samples with an applied potential of -300 mV. The protection afforded by the inhibitor is more noticeable in higher anodic potential range.

Table 8 - SCC testing in various concentrations of VCI 415 & tap water

| Alloy | VCI 415 | potential | Tensile strength (psi) | Strain _{failure} |
|-------|---------|-----------|------------------------|---------------------------|
| 7075 | 5% | -700 mV | 81078 | 0.104 |
| 7075 | 5% | -600 mV | 82771 | 0.104 |
| 7075 | 5% | -500 mV | 82993 | 0.100 |
| 7075 | 5% | -400 mV | 80730 | 0.092 |
| 7075 | 5% | -300 mV | 80777 | 0.082 |
| 7075 | 0% | -700 mV | 82198 | 0.100 |
| 7075 | 0% | -600 mV | 81218 | 0.100 |
| 7075 | 0% | -500 mV | 78795 | 0.084 |
| 7075 | 0% | -400 mV | 78802 | 0.074 |
| 7075 | 0% | -300 mV | 81831 | 0.064 |
| Alloy | VCI 415 | potential | Tensile strength (psi) | Strain _{failure} |
| 2024 | 5% | -700 mV | 70032 | 0.109 |
| 2024 | 5% | -600 mV | 68934 | 0.106 |
| 2024 | 5% | -500 mV | 69004 | 0.104 |
| 2024 | 5% | -400 mV | 72346 | 0.103 |
| 2024 | 5% | -300 mV | 67643 | 0.089 |
| 2024 | 0% | -700 mV | 71305 | 0.108 |
| 2024 | 0% | -600 mV | 75079 | 0.108 |
| 2024 | 0% | -500 mV | 74116 | 0.102 |
| 2024 | 0% | -400 mV | 68740 | 0.074 |
| 2024 | 0% | -300 mV | 70344 | 0.065 |
| Alloy | VCI 415 | potential | Tensile strength (psi) | Strain failure |
| 6061 | 5% | -700 mV | 51006 | 0.096 |
| 6061 | 5% | -600 mV | 51754 | 0.096 |
| 6061 | 5% | -500 mV | 50060 | 0.095 |
| 6061 | 5% | -400 mV | 50745 | 0.089 |
| 6061 | 5% | -300 mV | 51212 | 0.087 |
| 6061 | 0% | -700 mV | 50694 | 0.095 |
| 6061 | 0% | -600 mV | 51099 | 0.094 |
| 6061 | 0% | -500 mV | 47507 | 0.092 |
| 6061 | 0% | -400 mV | 50901 | 0.081 |
| 6061 | 0% | -300 mV | 47955 | 0.071 |

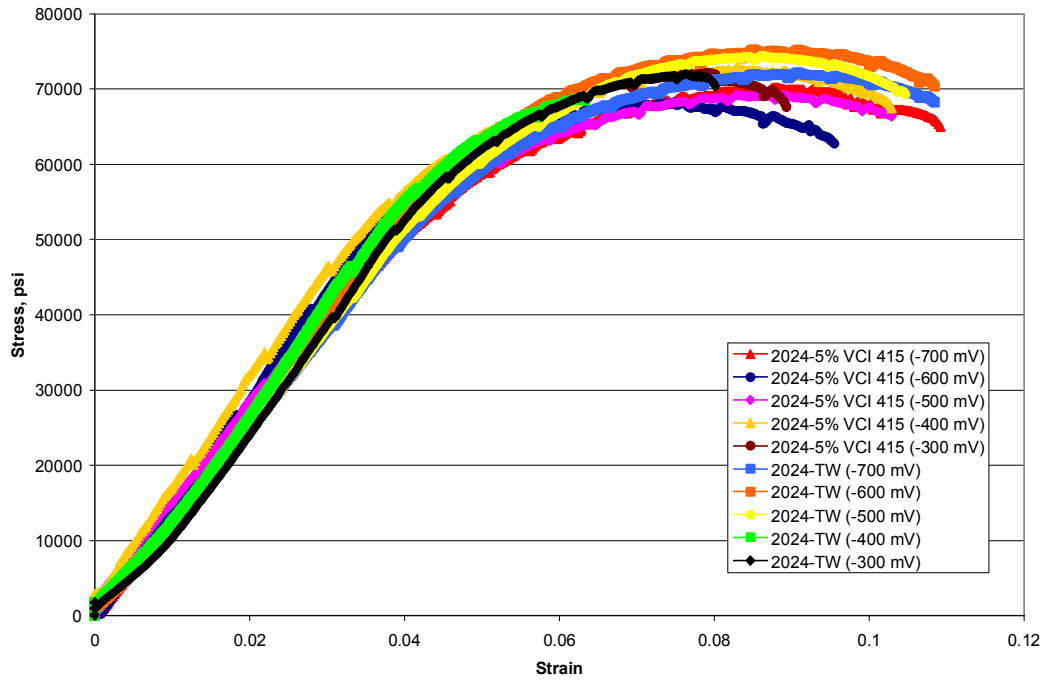


Figure 10: Stress/strain curves from SCC tests compare behavior for Al-2024 with and without inhibitor and applied potentials.

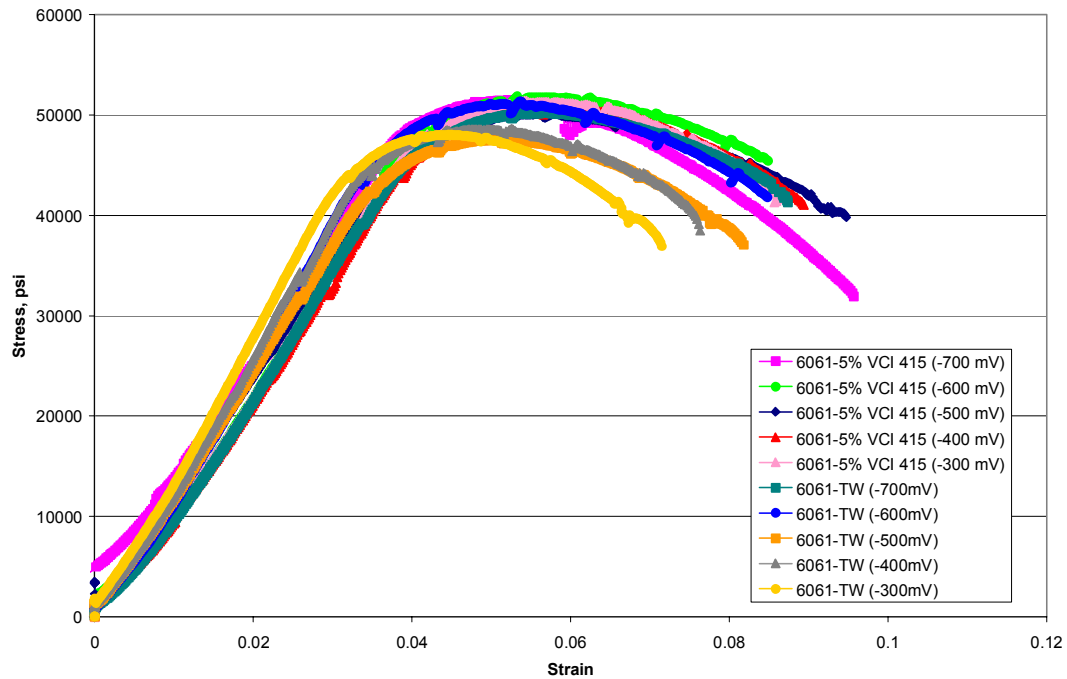


Figure 11: Stress/strain curves from SCC tests compare behavior for Al-6061 with and without inhibitor and applied potentials.

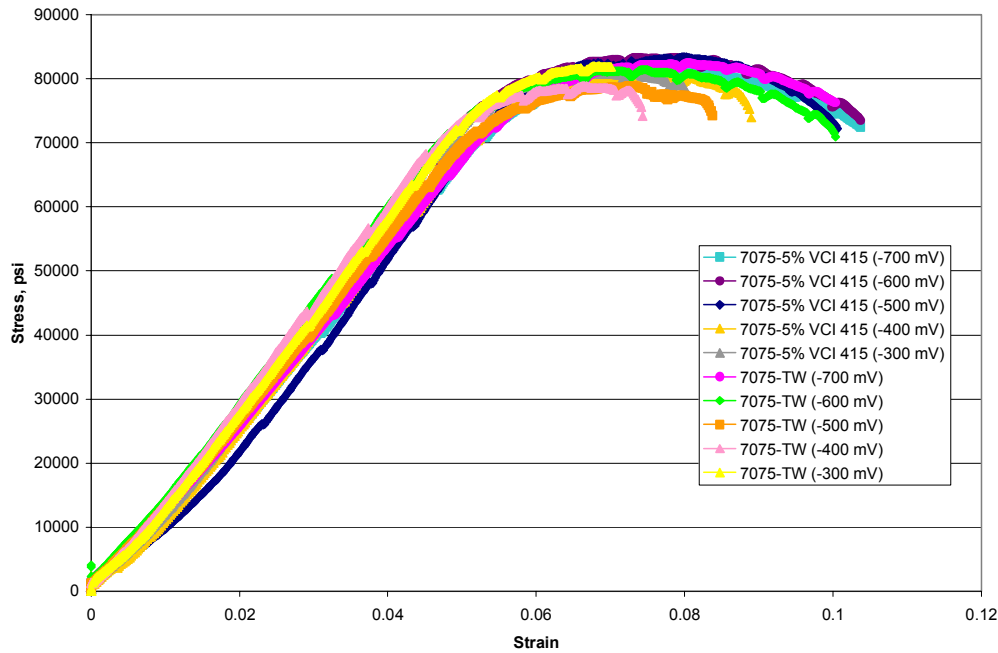


Figure 12: Stress/strain curves from SCC tests compare behavior for Al-7075 with and without inhibitor and applied potentials.

Analysis

Susceptibility to SCC was determined for the three alloys. At potentials exceeding breakdown, a noticeable increase in susceptibility is seen for the samples tested in tap water without inhibitor in Figures 13-15. The closer the value is to 1.0 on the y-axis, the less susceptible the alloy is to SCC. The greatest reduction in degree of susceptibility is seen around -300mV. The data acquired from the EIS tests show that VCI 415 increases the polarization resistance (R_p) value of the samples. It is assumed that the extremely high R_p value (in the range of a hundred thousand ohms) is due to the progressive film formation on aluminum. At higher VCI concentrations, this film could be seen with the naked eye. The data obtained from the EIS experiment best fit the Langmuir adsorption isotherm, where $\ln C$ vs. $[\ln \theta - \ln (1-\theta)]$ resulted in good linearity as seen in Figure 16. The thermodynamics of adsorption can provide valuable information about the mechanism of inhibition. The important thermodynamic values (changes in enthalpy of adsorption and changes in free standard energy of adsorption) can be obtained with adsorption isotherms and classical thermodynamics. The value of ΔG_{ad} is very important for the identification of an adsorption mechanism. In chemisorption (chemical adsorption), ΔG_{ad} is usually much higher than physisorption (physical adsorption). The criterion for chemisorption varies, for example, Bridka has suggested that chemisorption requires about -100 kJ/mol energy, whereas Metikos-Hukovic believes that chemisorption needs about -40 kJ/mol energy [31]. Still others assert that physisorption requires energy between -5 to -20 kJ/mol. ΔH_{ad} also plays an important role in the identification of an adsorption mechanism [23]. Chemisorption makes strong bonding between a chemical and the surface that the chemical has been applied to.

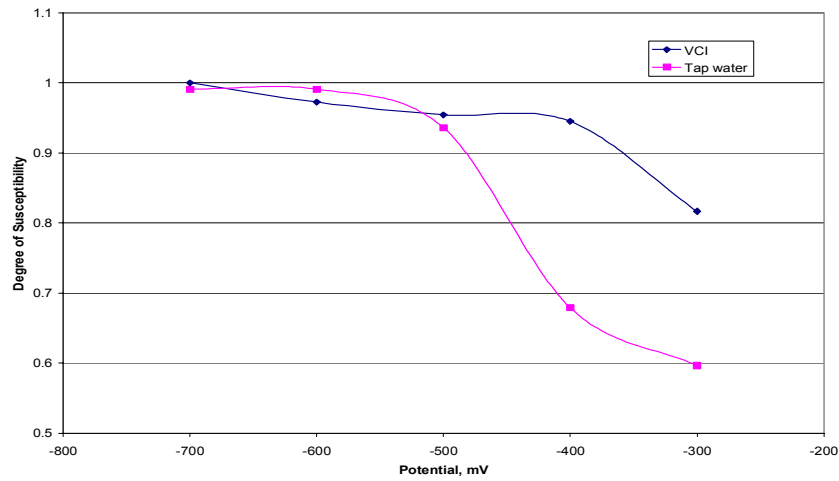


Figure 13: SCC susceptibility of Al-alloy 2024.

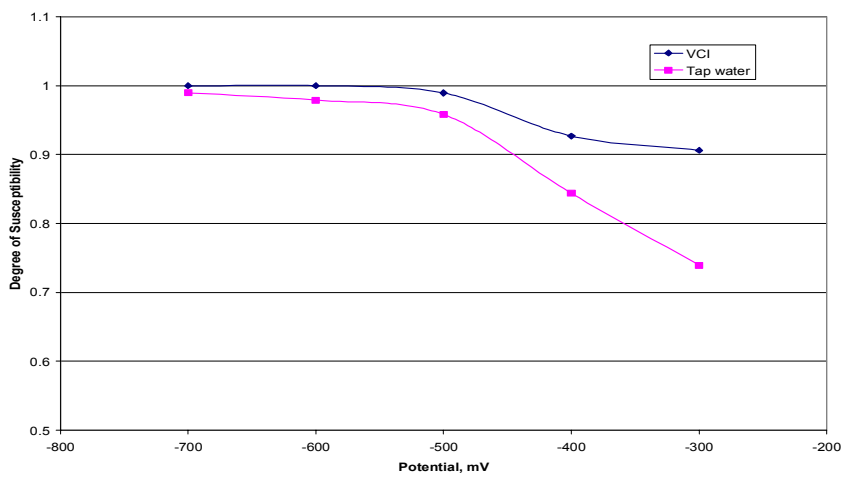


Figure 14: SCC susceptibility of Al-alloy 6061.

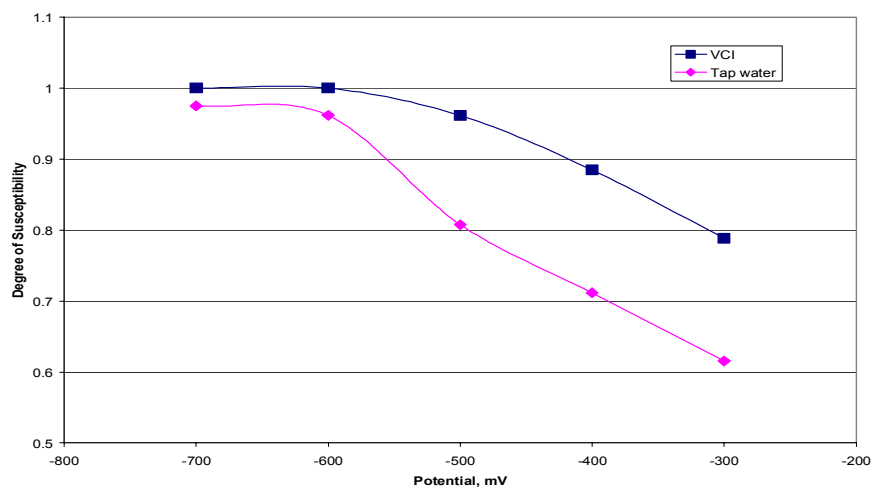


Figure 15: SCC susceptibility of Al-alloy 7075.

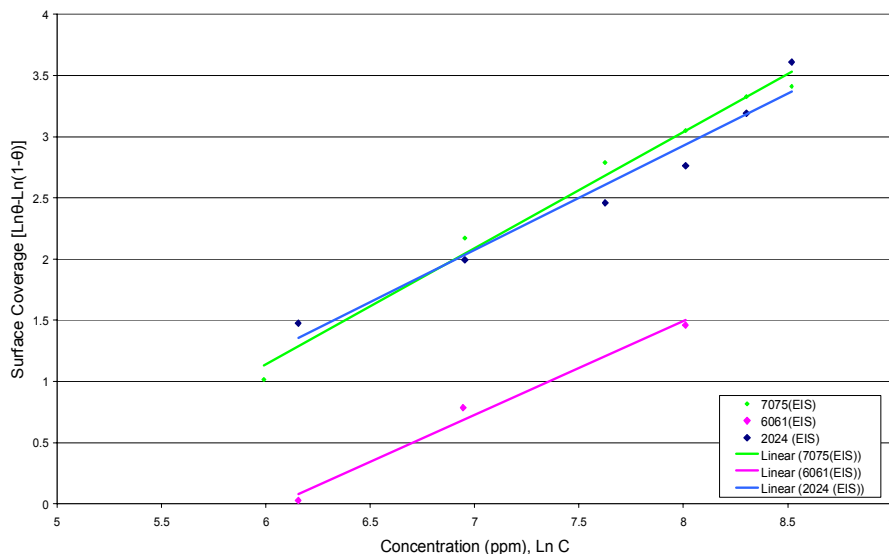


Figure 16: Langmuir adsorption isotherm showing the relationship between surface coverage and concentration.

X-ray Photoelectron Spectroscopy

7075 Al alloy samples were coated with VCI inhibitor, air dried and placed in the vacuum chamber of a Kratos Axis Ultra for examination. From the XPS analysis (hybrid lens mode, pass energy of 80, Al monochromatic anode, step rate of 1000 meV, dwell time of 60 ms), Figures 17-19 were obtained. Figure 17 shows the VCI 415 chemical composition is a mixture of sodium compounds and hydrocarbon surfactant. Figure 18 shows the same uniform chemistry at different locations; each colored curve represents a separate sweep of the surface. Figure 19 and Table 9 provide information for the depth profile beginning at the surface and etching away layers of material for roughly 180 second intervals. At the end of each etch cycle, the composition was determined. The final scan is seen at the front of the graph. The chemical components remain constant throughout the depth profiling, but the surfactant concentration increased slightly with etching (closer to the metal surface). Initially, it was thought the product contained an excess of sodium hydroxide that served as a pH adjuster. From electrochemical testing, however, there was visible evidence of film formation on the surface of the Al alloy.

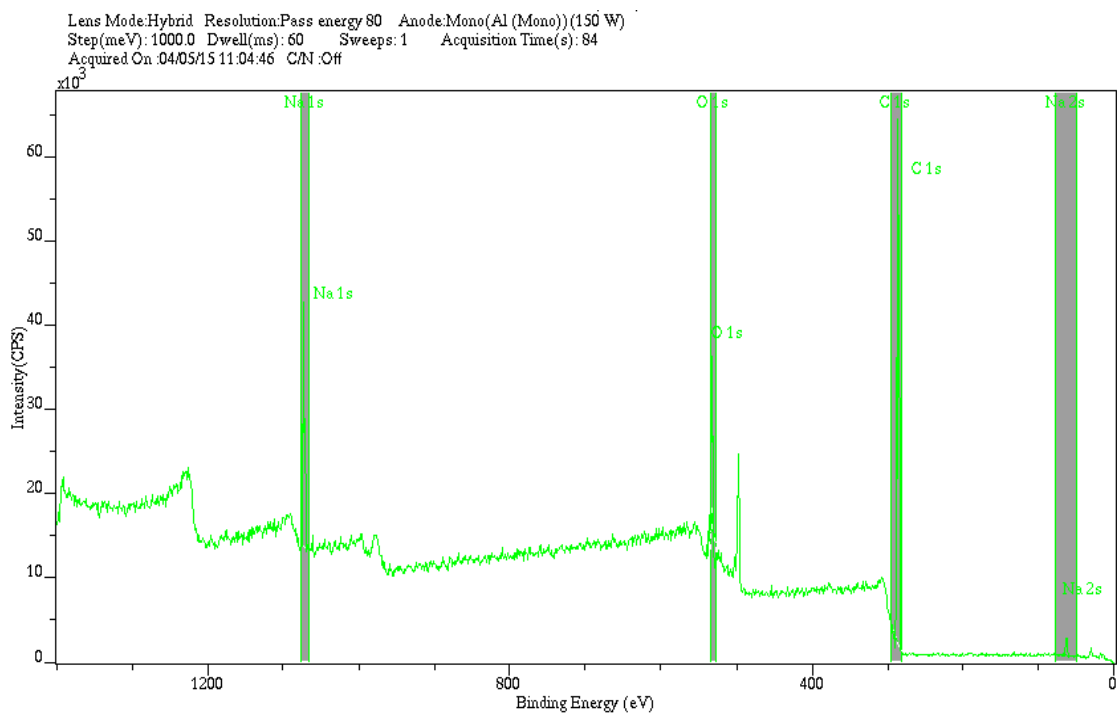


Figure 17: XPS analysis shows the VCI 415 chemistry contains sodium compounds and hydrocarbon surfactants.

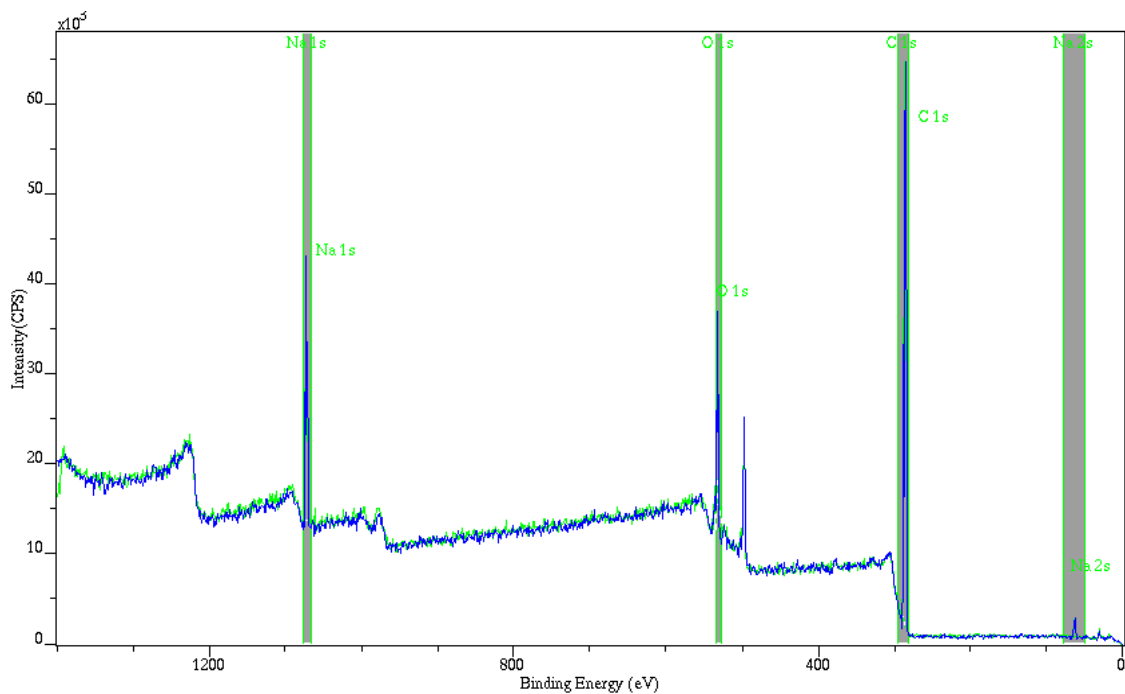


Figure 18: XPS analysis of the VCI 415 inhibitor shows uniform chemistry of sodium compounds and hydrocarbon surfactants at different locations.

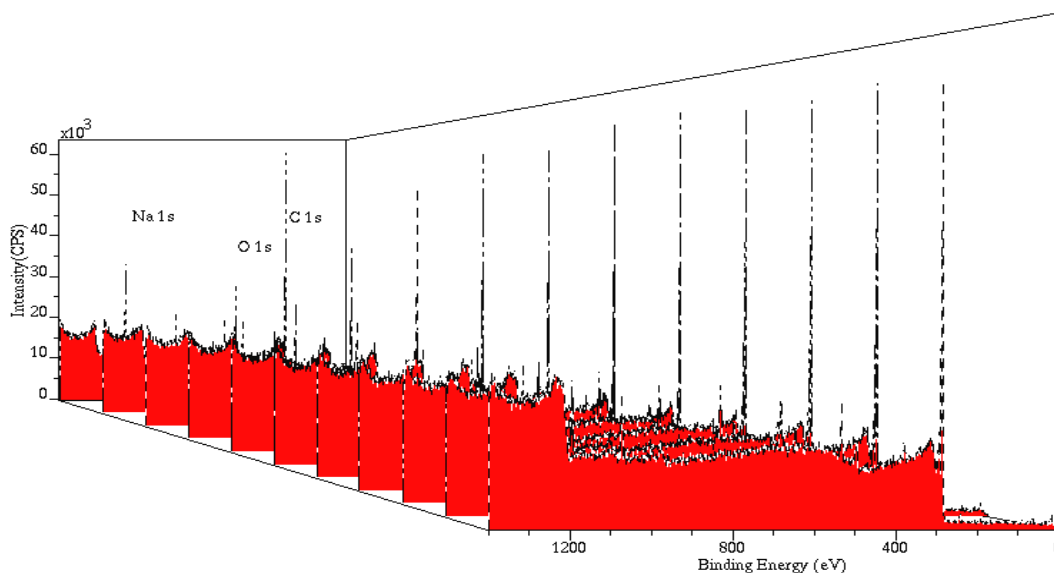
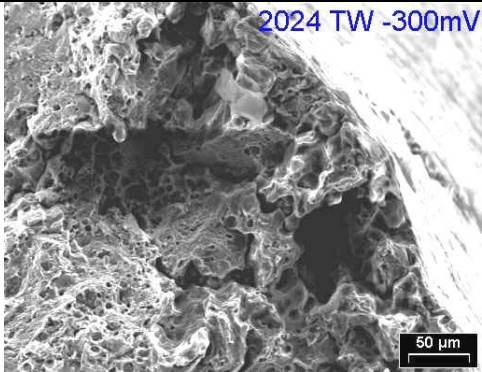
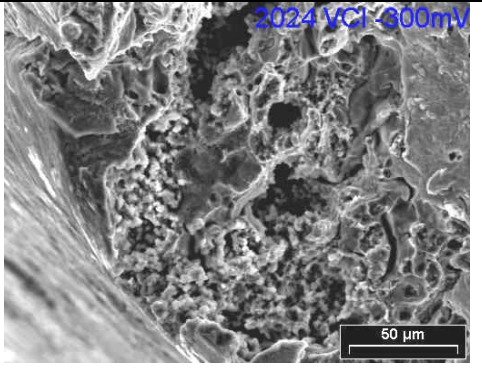
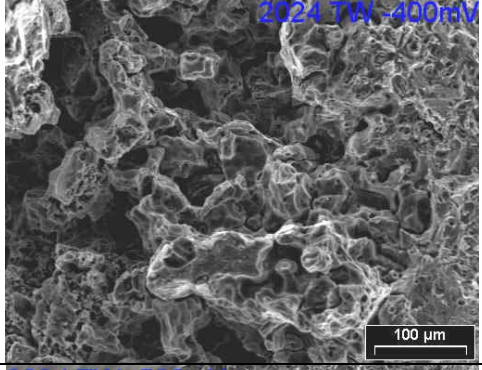
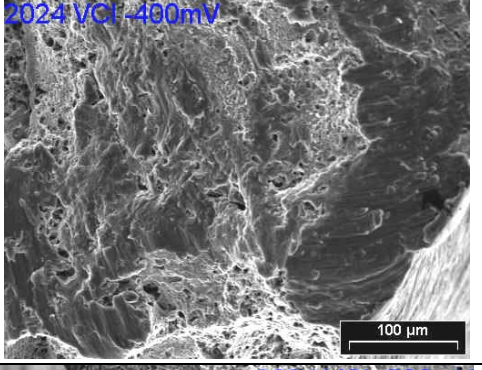
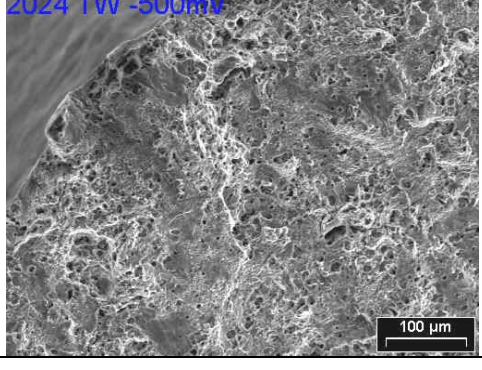
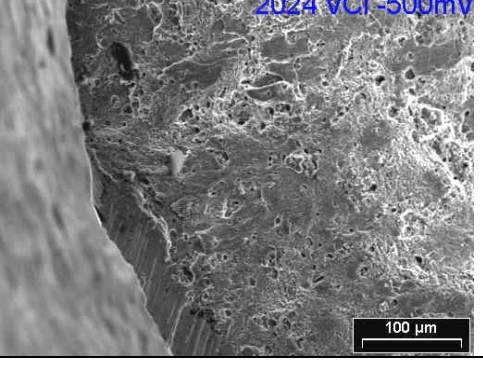


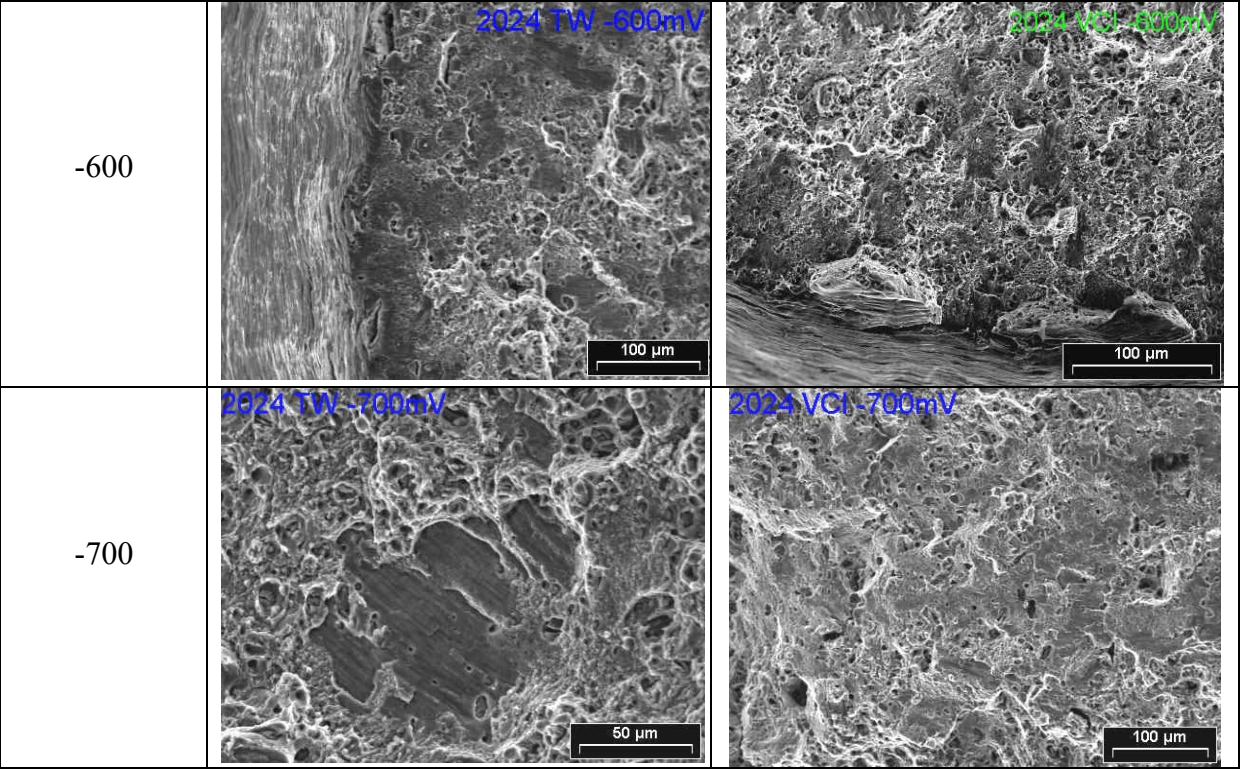
Figure 19: Depth profile for VCI 415 on 7075 Al-alloy substrate. Surfactant chemistry is predominant closer to the metal surface.

| Table 9 – Depth profile for VCI 415 on 7075 Al-alloy substrate. | | | | | | | |
|---|---------------------|--------------|---------------------|-------|----------------|-----------------|---------------|
| Peak | Position BE (eV) | FWHM (eV) | Raw Height (CPS) | RSF | Atomic Mass | Atomic Conc% | Mass Conc% |
| State #0 : Etch Time 0.00 seconds | | | | | | | |
| Na 1s | 1073.000 | 2.027 | 22174.7 | 1.685 | 22.990 | 4.62 | 8.25 |
| O 1s | 533.000 | 2.377 | 17908.9 | 0.780 | 15.999 | 8.94 | 11.11 |
| C 1s | 287.000 | 1.901 | 58630.8 | 0.278 | 12.011 | 86.44 | 80.64 |
| State #1 : Etch Time 180.00 seconds | | | | | | | |
| Na 1s | 1073.000 | 2.626 | 10307.1 | 1.685 | 22.990 | 2.61 | 4.79 |
| O 1s | 534.000 | 3.360 | 10757.7 | 0.780 | 15.999 | 6.54 | 8.33 |
| C 1s | 285.000 | 2.786 | 50578.9 | 0.278 | 12.011 | 90.84 | 86.88 |
| State #2 : Etch Time 360.00 seconds | | | | | | | |
| Na 1s | 1073.000 | 2.702 | 10250.6 | 1.685 | 22.990 | 2.56 | 4.73 |
| O 1s | 534.000 | 4.316 | 6693.5 | 0.780 | 15.999 | 4.01 | 5.15 |
| C 1s | 285.000 | 2.693 | 52822.6 | 0.278 | 12.011 | 93.43 | 90.12 |
| State #3 : Etch Time 600.00 seconds | | | | | | | |
| Na 1s | 1073.000 | 2.842 | 8118.4 | 1.685 | 22.990 | 2.09 | 3.87 |
| O 1s | 533.000 | 3.725 | 6429.6 | 0.780 | 15.999 | 3.96 | 5.11 |
| C 1s | 285.000 | 2.714 | 51620.0 | 0.278 | 12.011 | 93.95 | 91.02 |

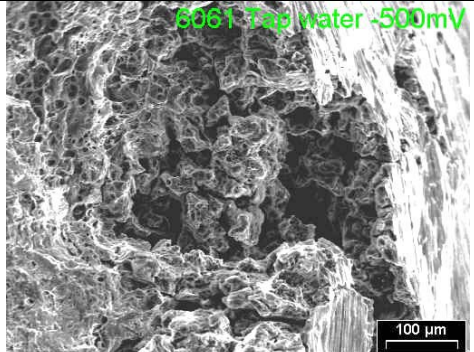
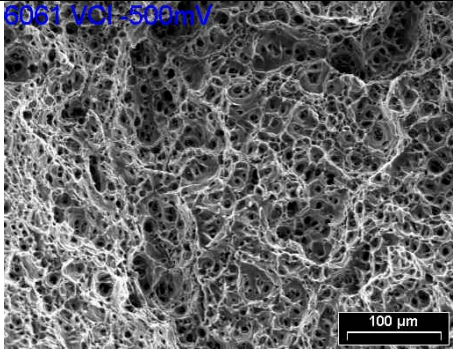
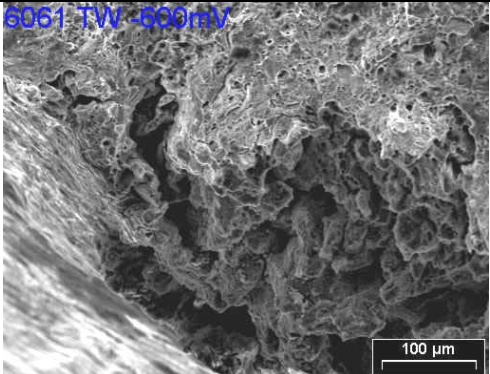
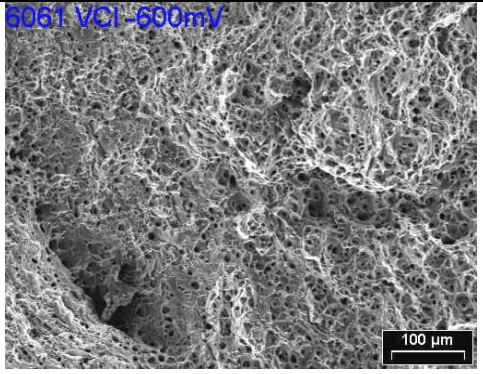
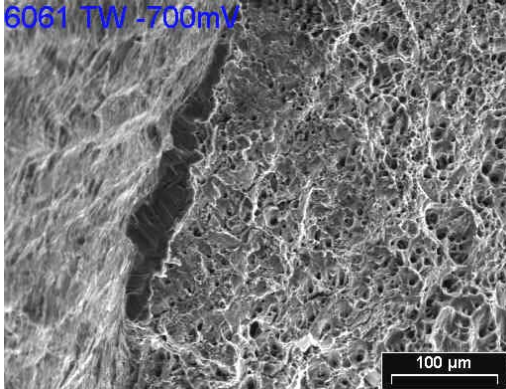
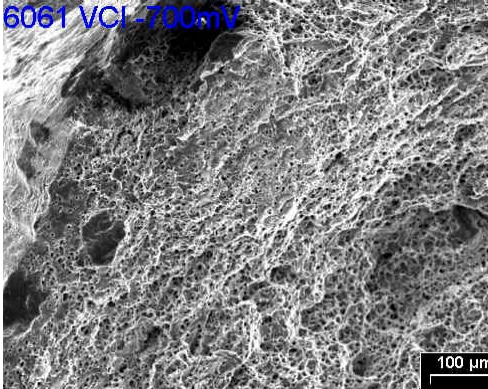
Tables 10–12 show the SEM photographs from the SCC testing. These photos demonstrate greater susceptibility to SCC for samples tested in tap water without inhibitor. Examination of the failed samples revealed some damage for all Al-alloys in both testing conditions at the more aggressive potentials (-300 mV and -400 mV). The SEM fractographs provide evidence of the worst damage areas seen on the samples, typically at the edges. Evidence of SCC attack was seen at potentials of -300 mV and

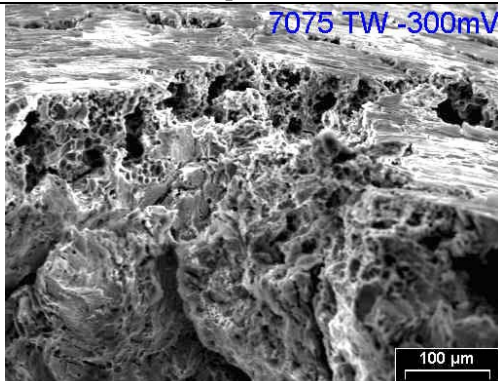
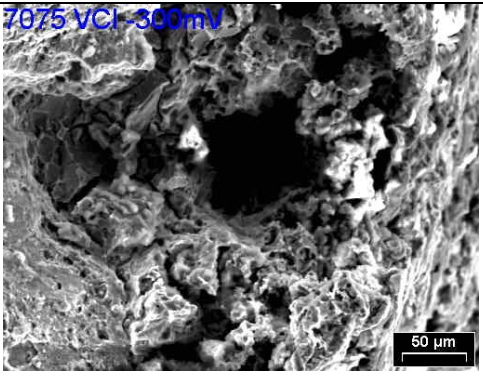
-400 mV for Al-2024 samples, which is consistent with the polarization behavior from Figure 1. Also corroborating this is the large difference seen in the strain at failure (Table 8) for -400 mV 5% VCI and 0% VCI. For Al-6061, SCC attack was seen at all potential levels for the untreated specimen, however very minor damage at -700 mV. The SEM photos for Al-7075 showed minor levels of SCC attack and pitting corrosion at the edges. In general, the morphology of the samples tested in tap water showed more intergranular localized corrosion. Samples tested in VCI 415 showed a typical ductile overload failure with no localized corrosion damage except at aggressive potentials in the -300 and -400 mV range.

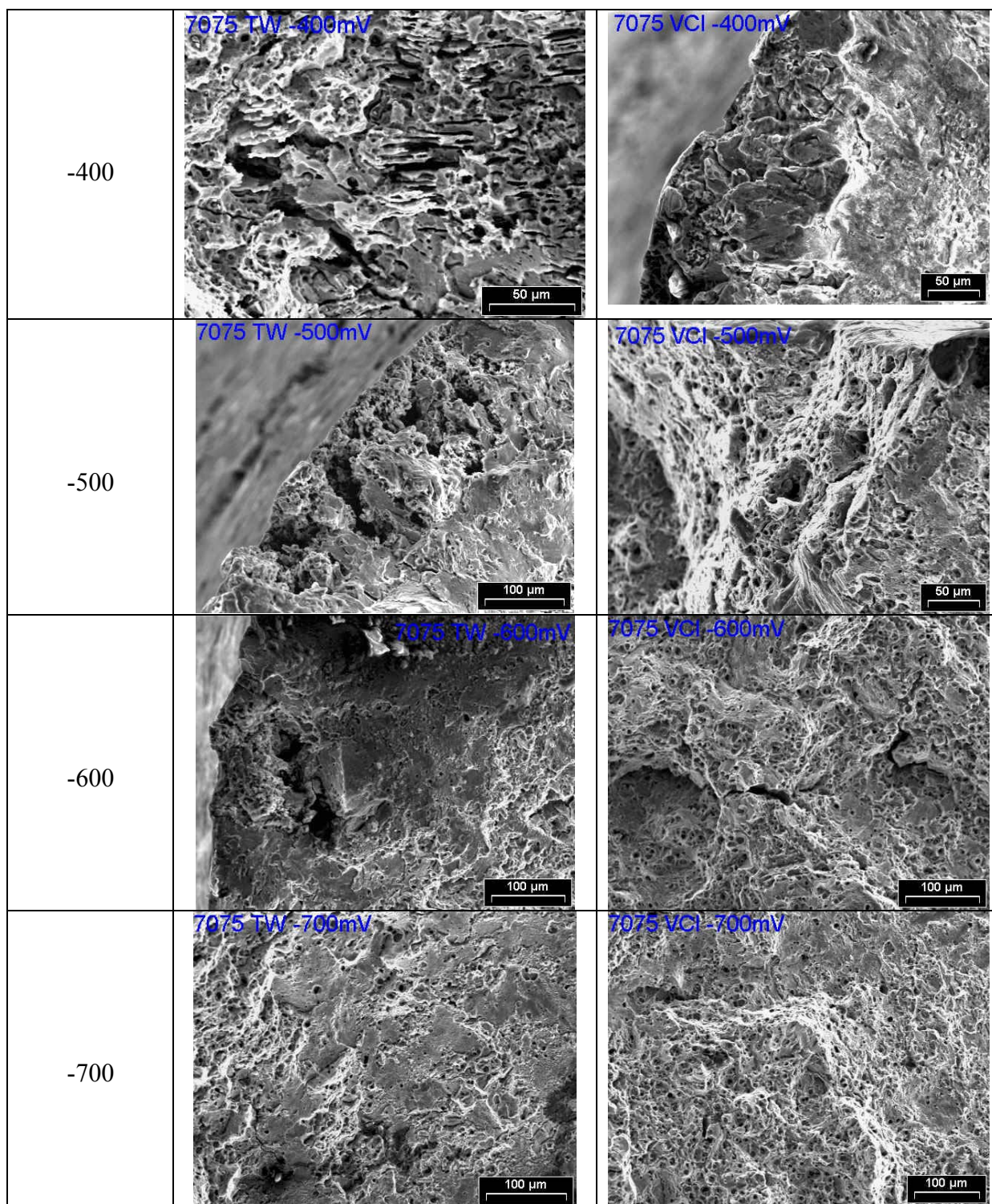
| Table 10 – SEM photos of the fracture surface for Al-2024 with different applied potentials. | | |
|--|---|---|
| Potential (mV) | Tap water | VCI |
| -300 |  <p>2024 TW -300mV</p> |  <p>2024 VCI -300mV</p> |
| -400 |  <p>2024 TW -400mV</p> |  <p>2024 VCI -400mV</p> |
| -500 |  <p>2024 TW -500mV</p> |  <p>2024 VCI -500mV</p> |



| Table 11 – SEM photos of the fracture surface for Al-6061 for each applied potential. | | |
|---|--|--------------------------------------|
| Potential (mV) | Tap water | VCI |
| -300 | <p>6061 TW -300mV</p> <p>100 μm</p> | <p>6061 VCI -300mV</p> <p>50 μm</p> |
| -400 | <p>6061 Tap water -400mV</p> <p>100 μm</p> | <p>6061 VCI -400mV</p> <p>100 μm</p> |

| | | |
|------|--|--|
| -500 |  <p>6061 Tap water -500mV</p> |  <p>6061 VCI -500mV</p> |
| -600 |  <p>6061 TW -600mV</p> |  <p>6061 VCI -600mV</p> |
| -700 |  <p>6061 TW -700mV</p> |  <p>6061 VCI -700mV</p> |

| Table 12 – SEM photos of the fracture surface for Al-7075 with different applied potentials. | | |
|--|---|---|
| Potential (mV) | Tap water | VCI |
| -300 |  <p>7075 TW -300mV</p> |  <p>7075 VCI -300mV</p> |



Conclusion

A comprehensive investigation was undertaken to characterize the corrosion behavior of aircraft Al alloys (2024-T3, 6061-T6, 7075-T6) in a vapor phase corrosion inhibitor used for washing/rinsing aircraft. Alternate immersion tests resulted in severe crevice corrosion and discoloration for samples tested without inhibitor. Samples tested in 5% and 10% VCI 415 solutions showed far less corrosion damages. The VCI 415 chemical composition is a mixture of sodium compounds and hydrocarbon surfactant with uniform chemistry across the surface and minor variation of concentration with depth. Initially, it was thought the product contained an excess of sodium hydroxide that served as a pH adjuster. From electrochemical testing, however, there was visible evidence of film formation on the surface of the Al alloy. The polarization resistance of the samples increased with the concentration of VCI 415, due to the film forming process and displacement of water molecules by a hydrophobic head.

Effectiveness of the inhibitor was confirmed with electrochemical impedance spectroscopy and elevated temperature studies. As well, identification of the adsorption mechanism and corrosion activation energy was explored. The data acquired from EIS tests showed that adsorption of VCI 415 to the high strength aluminum alloys fits with the Langmuir adsorption isotherm. XPS analysis showed strong carbon bonding, further corroborating the adsorption isotherm calculations. Cyclic polarization behavior for samples in the vapor phase inhibitor showed a shift in the passive film breakdown potential by roughly +600 mV. This dramatic increase in the passivation range will reduce pitting and improve localized cell chemistry. Crevice corrosion test results showed improved corrosion inhibition behavior compared with samples tested in tap water only. The strain at failure and tensile strength from the stress corrosion cracking studies showed pronounced effects at -300mV; the greatest improvements are seen for the samples tested with VCI 415. Furthermore, improved fractographic morphology was observed for the alloys tested in the inhibitor solution; ductile overload was the primary failure mode.

In summary, this modified aircraft wash with VCI 415 inhibitor demonstrates an effective protective film on the surface of aluminum alloys with no adverse effects from the alkaline chemistry, and can contribute to improving durability for aircraft structures.

References

- [1] Aviation Week Newsletters, the Aviation & Aerospace Almanac, GKMG Consulting Services, Inc., 1999.
- [2] <http://www.corrosioncost.com/pdf/aircraft.pdf>
- [3] J. A. Marceau, "Service Experience with Current (Aging) Fleet," Presentation to the Committee on New Materials for Advanced Civil Aircraft, National Materials Advisory Board, National Research Council, Washington, D.C., September 28, 1994.
- [4] J. A. Marceau, "Regarding corrosion control and aging aircraft," presented at the 2nd Annual International Conference on Aging Aircraft, October 3-5, Baltimore, Md. Washington, D.C., Federal Aviation Administration, 1989.
- [5] J. T. Staley, "Aluminum alloys in subsonic aircraft," presented at the Second Thermal Structures Conference, Charlottesville, Va. E. Thornton, ed. Washington, D.C., American Institute of Aeronautics and Astronautics, 1994.

- [6] E.A. Starke and J.T. Staley, "Application of modern aluminum alloys to aircraft," Progress in Aerospace Sciences, 1996.
- [7] http://amptiac.alionscience.com/pdf/AMPQ5_4.pdf
- [8] <http://www.key-to-metals.com/Article95.htm>
- [9] Stress corrosion cracking of aluminum alloys
<http://www.key-to-metals.com/ViewArticle.asp?ID=17>
- [10] Metals Handbook, 10th Ed., Vol. 11, Failure Analysis and Prevention, ASM International, Materials Park, Ohio, 2002.
- [11] Metals Handbook, 9th Ed., Vol. 13, Corrosion, ASM International, Materials Park, Ohio, 1987.
- [12] <http://www.alu-info.dk/Html/alulib/modul/A00118.htm>
- [13] <http://www.materialsengineer.com/G-Crevice-Corrosion.htm>
- [14] Bull. Mater. Sci., Vol. 23, No. 1, February 2000, pp. 47–49. © Indian Academy of Sciences.
- [15] <http://www.epa.gov/compliance/resources/publications/assistance/sectors/notebooks/>
- [16] M. R. Saleh, A.M. Shams El Din, Corros. Sci. 12 (1981) 688.
- [17] <http://www.vciproblems.com/>
- [18] A. Eydelnant, B. Miksic, "Use of Volatile Inhibitors (VCIs) For Aircraft Protection, 6/30/98.
- [19] <http://www.cortecvci.com/Publications/Papers/VCIProducts/CTP-3.PDF>
- [20] http://www.surfactantseurope.akzonobel.com/cleaning/brochures/Berol_260_266_and_840_Narrow_range_ethoxylates.pdf
- [21] M. L. Free, "A new corrosion inhibition model for surfactants that more closely accounts for actual adsorption than traditional models that assume physical coverage is proportional to inhibition," Corrosion Science, In Press, Corrected Proof, 10 May 2004.
- [22] M. Lagrenée, B. Mernari, M. Bouanis, M. Traisnel and F. Bentiss, "Study of the mechanism and inhibiting efficiency of 3,5-bis(4-methylthiophenyl)-4H-1,2,4-triazole on mild steel corrosion in acidic media," Corrosion Science, Vol 44, Issue 3, March 2002.
- [23] W. Durine, R. D Marco, A. Jefferson, and B. Kinsella, Journal of the Electrochemical Society, 146 (5) 1751-1756 (1999)
- [24] G61-86(2003) Standard Test Method for Conducting Cyclic Potentiodynamic Polarization Measurements for Localized Corrosion Susceptibility of Iron-, Nickel-, or Cobalt-Based Alloys, ASTM International.
- [25] http://www.gamry.com/App_Notes/EIS_Primer/EIS_Primer.htm
- [26] ASTM G44-99, "Standard Practice for Exposure of Metals and Alloys by Alternate Immersion in Neutral 3.5% Sodium Chloride Solution," ASTM International.
- [27] ASTM G47-98(2004) Standard Test Method for Determining Susceptibility to Stress-Corrosion Cracking of 2XXX and 7XXX Aluminum Alloy Products ASTM International.
- [28] <http://www.kratos.com/Agan/SMA.html>
- [29] <http://www.chem.qmw.ac.uk/surfaces/scc/>
- [30] <http://www.thermovgscientific.com/>
- [31] R. Gasparac, C. R. Martin and E. Stupnisek-Lisac, "In situ Studies of Imidazole and its Derivatives as Copper Corrosion Inhibitors," Journal of The Electrochemical Society, 147 (2) 548-551 (2000).